FEATURE ARTICLE

Helium Cluster Isolation Spectroscopy of Alkali Dimers in the Triplet Manifold

J. Higgins, C. Callegari, J. Reho, F. Stienkemeier,[§] W. E. Ernst,[†] M. Gutowski,[‡] and G. Scoles*

Department of Chemistry, Princeton University, Princeton, New Jersey 08544

Received: February 12, 1998; In Final Form: April 22, 1998

Helium cluster isolation spectroscopy is a recently developed spectroscopic method that involves the formation of a beam of large helium clusters (10^4 atoms per cluster), the capture by the clusters of the atoms or molecules of interest in a low-pressure pick-up cell, and the spectroscopic study of the isolated species. Here we exploit the unique feature of this method of allowing the selective preparation of high-spin molecular species (e.g., triplet dimers) over their low-spin (singlet) counterparts to measure the spectra of several alkali dimers in their triplet manifold. By probing via laser-induced fluorescence their lowest triplet-to-triplet transitions, Li_2, Na_2, K_2, and NaK are found to reside on the surface of the helium clusters. Since the spectroscopic shifts induced by the helium cluster are minimal, vibrational analysis of the electronic transitions produces transition frequencies that can be compared to previous ab initio and experimental values. Both bound−bound and bound−free transitions have been observed. Emission spectra reveal the presence of vibrational relaxation and nonadiabatic intersystem crossings of the excited dimers that result from the proximity of the helium cluster surface. Through this study we improve our understanding of triplet alkali dimer potential energy curves, we test an efficient analytical model to represent them, and we provide input information for the study of nonadditive effects present in quartet (spin-polarized) alkali trimers which can be formed using the same method.

I. Introduction

The spectroscopy of dimers has traditionally provided the most accurate results on the negative part of the interaction potential between atoms. Detailed mapping of the potential energy curves in the ground and excited states provides insight into the nature of bonding and the intermolecular forces. The single valence electron structure of alkali metal atoms produces a simple bonding scheme for their dimers in that the nature of the bond (covalent or van der Waals) is determined only by the spin configuration of the single electron pair that participates in the bonding. This has allowed high-level electronic structure calculations that provide reasonably accurate potential energy surfaces for the ground and excited states of these species.[1,2] However, the accuracy of the calculations falls off rapidly as the atomic weight of the atom increases, due to the increased importance of relativistic and valence−core correlation effects.

Using the technique of helium cluster isolation, the spectroscopy of spin-polarized alkali trimers has recently been shown to be both feasible and useful for gaining insight into many-body interactions in van der Waals systems.[3] As a required step toward developing a comprehensive understanding of intermolecular forces in general and of many-body effects in small clusters made of metal atoms, we present here a systematic study of two-body interactions between alkali atoms in the triplet manifold carried out using the same technique.

A. Spectroscopy of the Alkali Dimers. The singlet states of the alkali dimers, in particular Na_2, have been extensively observed and characterized since the first work by Roscoe and Schuster in 1874.[4] An excellent review of the early work on Na_2 up to 1981 is given in ref 5. More recent work on the singlet states of Na_2 has involved the detailed, high-precision analysis of the low-lying states.[6] In addition, there has been much effort directed at the characterization of high-lying Rydberg states of the Na_2 molecule.[7] The study of the triplet electronic states has proven to be more elusive since the strongly bound singlet dimers will preferentially form both in an atomic vapor-filled cell and in a molecular beam expansion. Access to the triplet manifold of electronic states was first gained by spin−orbit perturbations of singlet states by nearby triplet electronic states. Mixing of the levels makes transitions involving $\Delta S \neq 0$ possible. It is through this method that much work has been done on the mapping of the potential energy curves of the triplet manifold of both the homonumclear and heteronuclear alkali dimers. The potential energy curves for the low-lying electronic states in the singlet and triplet manifolds of Na_2[8] are displayed in Figure 1. Fluorescence resulting from the excitation of mixed levels has lead to the observation of the lowest triplet states of the alkali dimers.[9−11] The development of double and triple resonance techniques has provided a wealth of information on the high excited states in the triplet manifold all the way up to the Rydberg levels.[12,13]

* To whom correspondence should be addressed.

[§] Present address: Fakultät für Physik, Universität Bielefeld, D-33615 Bielefeld, Germany.

[†] On sabbatical from the Department of Physics, Pennsylvania State University, University Park, PA 16802.

[‡] Solid State Theory Group, Materials and Chemical Sciences, Pacific Northwest National Laboratory, Richland, WA 99352, and Department of Chemistry, University of Gdańsk, 80-952 Gdańsk, Poland.

S1089-5639(98)01115-3 CCC: $15.00
Published on Web 06/05/1998

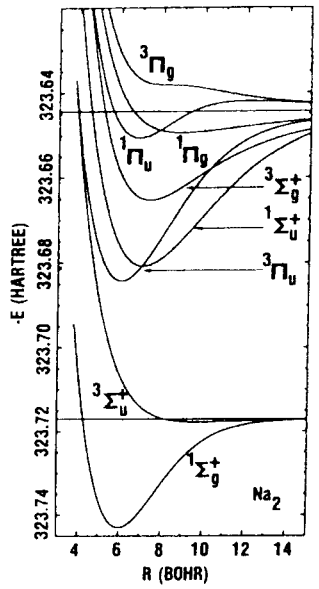

Figure 1. Potential energy curves for the singlet and triplet manifolds of Na_2 that correlate to the 3s+3s and 3s+3p asymptotes of Na_2.[8]

The work presented here differs from that based on perturbation-facilitated spectroscopy in that access to the triplet manifold of the alkali dimers is provided by directly preparing dimers in the state of interest using the technique of helium cluster isolation spectroscopy. As it will be shown below, this method can be used to selectively produce triplet dimers in greater abundance than the corresponding singlet states. Only two examples are present in the literature of triplet dimer spectroscopy carried out by excitation of the lowest triplet state prepared directly in a molecular beam.[14] In a free jet beam source the situation is opposite of that occurring in our setup in that the supersonic expansion will predominantly form singlet ground state molecules, allowing only a small quantity of triplet states to be produced.

B. Helium Cluster Isolation Spectroscopy. Several methods are currently being developed to carry out spectroscopic measurements at very low temperatures. These include photoassociative spectroscopy of laser-cooled and trapped atoms,[15] helium buffer gas cooling and magnetic trapping of paramagnetic atoms and molecules,[16] and the subject of this article: spectroscopy of atoms and molecules trapped in or on liquid helium clusters.[17−21]

Helium clusters are the only atomic clusters that are definitely known to be liquid since helium will solidify only under pressure. They attain very low temperatures (0.4 K[20,22]) and may be superfluid (at least the larger clusters[21,22]). Since direct measurement of the physical properties of the pure helium clusters has proven difficult to this point, various chromophores have been attached to the clusters to probe them. If a chromophore is chosen such that its spectroscopy in the gas phase is known, any perturbation induced by the presence of the helium cluster can be easily quantified. SF_6 was the first chromophore used to this end. The low-resolution infrared spectrum of the ν_3 band of SF_6 was studied by Goyal and co-workers[23] in 1992. The limited line-by-line tunabilty of the CO_2 lasers used in the experiment did not allow resolution of the rotational structure of the transition. The experiment did show, however, that the spectroscopic shifts induced by the helium cluster medium are small and that the lines are relatively narrow. The ν_3 band of SF_6 was found to be shifted by no more than 1.5 cm^{-1} to the red of the gas-phase absorption, while the lines were found to be no wider than 18 GHz.[23]

A rotationally resolved infrared spectrum of the same band of SF_6 was recently obtained by Hartmann and co-workers.[20] The rotational constants of the solvated molecule were found to differ by almost a factor of 3 from their gas-phase values, and two possible explanations of this effect were proposed. In the first, the change was attributed to a synchronous motion of the SF_6 molecule and a shell of helium atoms surrounding it, while in the second the effect has been associated with the in-and-out motion of the He atoms produced by the rotation of the nonspherical potential field generated by the rotating SF_6 molecule.[20] The intensities of the lines were found to be consistent with a rotational temperature of 0.37 ± 0.05 K, which is in good agreement with the previously calculated value of 0.4 K[22] for clusters of ^{4}He. While a location of the SF_6 molecule on the surface of the cluster had been hypothesized in a previous work[23] from our group, the data of Hartmann et al.[20] provided conclusive evidence for the location of the SF_6 inside the large helium cluster. Previous calculations on SF_6-doped helium clusters had also predicted an interior state for the dopant molecule,[24] which follows from the fact that the binding of a helium atom to SF_6 is much greater than the helium−helium interaction energy. The situation is different for alkali atoms. In this case, the interaction energy between an alkali atom and helium[25] is much weaker than that between two helium atoms.[26] Calculations reveal that any alkali atom attached to a helium cluster remains on the cluster surface without becoming solvated.[27] This was confirmed in a series of experiments carried out in our laboratory.[28] The $nP_{3/2,1/2} \leftarrow nS_{1/2}$ atomic transitions of Li, Na, and K were studied by laser-induced fluorescence (LIF) spectroscopy. Two types of transitions were observed corresponding to the different orientations of the excited state alkali p orbital relative to the cluster surface. Excitation to states with the p orbital aligned perpendicular to the surface of the helium cluster causes the desorption of the alkali atom from the cluster and produces free atom fluorescence. Excitation to a parallel configuration produces instead a bound excited state and strongly red shifted fluorescence due to a Na*−He excimer which forms when a helium atom binds near the node of the excited-state p orbital of the sodium atom. Identical excitation spectra can also be obtained by monitoring the laser-induced beam depeletion of the alkali metal atom measured with a hot wire surface ionization detector located downstream from the cluster beam/laser beam crossing point.

Group 1A alkali dimers can exist in two states, singlet and triplet, resulting in a very simple bonding scheme. If the valence electron spins are oriented in a low-spin (antiparallel) configuration, a covalent chemical bond is formed between the two atoms. A high-spin (parallel) configuration of the valence electrons results instead in weaker van der Waals bonding. In the case of Na_2, while the singlet state is bound by 5942.6880 (49) cm^{-1},[29] the triplet state has a dissociation energy of only 161.17 cm^{-1}.[30] In a heat pipe or molecular beam expansion of alkali vapor, the singlet state of the akakli dimers will form in far greater abundance of the triplet state due to its greater stability.

We have found that when alkali dimers are formed on the surface of helium clusters, triplet states are detected in greater abundance than their singlet counterparts, in contrast to the situation found in a heat pipe. This can be explained by considering the details of the formation process. In our experiments, large liquid helium clusters collect very efficiently one or more alkali metal atoms by passing through pick-up cells which contain atomic alkali vapor. After the impact energy of an alkali atom is dissipated to the cluster and the latter cools

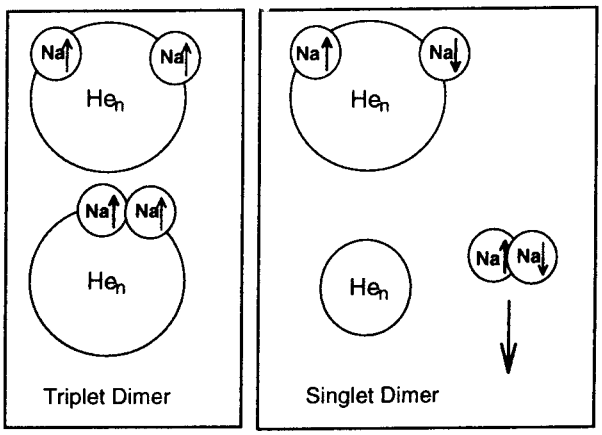

Figure 2. Schematic representation of the process for the formation of an alkali-triplet-enriched helium cluster beam. The doped helium cluster beam becomes enriched with triplet sodium dimers since the singlet species have a higher formation energy and therefore a higher probability of leaving the cluster surface because of the relaxation that follows the recombination.

by evaporation, the atom will be expelled by the liquid and will reside in a surface "dimple"[27] that consists of a small depression in the smooth density profile of the helium cluster surface. Under typical pick-up conditions, approximately 700 cm^{-1} of kinetic energy must be dissipated. If the helium cluster becomes doped with at least two atoms, they will eventually meet and form a dimer. If the atoms possess antiparallel electron spins and a singlet state ($1^1\Sigma_g^+$) is formed, the binding energy that is released causes heating of the cluster with the subsequent evaporation of helium atoms. Evaporation will cease once the cluster temperature has re-equilibrated to 0.4 K. If the atoms have parallel electron spins, the weakly bound triplet state ($1^3\Sigma_u^+$) will form. Assuming that the binding of a helium atom to a large cluster is 5 cm^{-1},[31] approximately 1150 He atoms need to evaporate after the formation of a singlet state, while only 35 will evaporate after a triplet state is formed. The dissipation of the greater binding energy of the singlet states may cause the desorption of the alkali molecule or the spreading of the cluster beam, or even the complete evaporation of the smaller clusters. The helium cluster beam then becomes enriched on axis with clusters doped with triplet dimers over and above the simple ehancement of 3:1, which is expected from the spin statistics. Triplet-state alkali dimers present in a helium cluster are expected to reside on its surface due to the similarity between the alkali atom−helium and the triplet dimer−helium interaction energies. Molecule formation via cluster pick-up appears to be a method for the selective preparation of weakly bound molecules over those that are bound by strong covalent bonds. A pictorial view of the above ideas is provided in Figure 2.

II. Experimental Section

Helium clusters ranging in average size up to 10^4 atoms per cluster are prepared in an expansion of helium gas through a 10 μm nozzle at temperatures ranging from 12−30 K and stagnation pressures of 3−10 MPa. At these source conditions, the $1/\sqrt{T}$ dependence of gas flux leads to a heavy gas load, which is removed by a 32 000 l/s diffusion pump. At such a low nozzle temperature, doping clusters with a chromophore cannot be achieved by coexpansion and the use of the pick-up seeding method[32] becomes necessary. The cluster beam passes through two collinear scattering cells located at a short distance after a 400 μm skimmer, where a pressure in the range of 10^{-3} to 10^{-1} Pa of the alkali of interest can be maintained. Colliding with a gas at these partial pressures, the helium clusters have a high probability of becoming doped with one or more alkali atoms. Typical cluster source conditions that lead to the production of the greatest number of doped clusters are 5 MPa stagnation pressure and 17.5 K nozzle temperature. The alkali vapor in the pick-up cells is supplied by two separated reservoirs through heated tubes. The temperature of the pick-up cells is maintained 100 K higher than that of the reservoir, avoiding alkali atom distillation and formation of dimers inside the cell. Dissipation of the energy following the chromophore attachment to the clusters is accomplished by evaporation of He atoms from the cluster. Evaporation ceases once the vapor pressure of the helium becomes negligible, which occurs when the cluster reaches a final temperature of less than 0.4 K.[22]

A few centimeters downstream, the doped clusters cross the output beam of a tunable continuous wave dye or titanium sapphire laser at the center of a two-mirror laser-induced fluorescence (LIF) collector. An optical fiber bundle transmits the emitted photons out of the vacuum apparatus. Excitation spectra are recorded by detecting the total emitted fluorescence with a cooled photomultiplier tube (Thorn-EMI 9863QB) operated in photon counting mode. Emission spectra are obtained using a monochromator (GCA/MacPherson model 700-51) coupled to a liquid nitrogen cooled charge-coupled device (Princeton Instruments model 1152UV). The laser frequency was measured using a home-built wavemeter with an absolute accuracy of 0.001 cm^{-1}, which was calibrated using the I_2 spectrum.

A Langmuir−Taylor surface ionization detector located after the LIF detector is used to measure the intensity of the alkali-doped cluster beam and obtain spectra based on beam depletion measurements. If the laser is tuned through an alkali absorption, a decrease in the surface ionization signal correlated to the cluster beam will be observed. In addition to fluorescence, absorption of a photon by an alkali atom or molecule results in either chromophore desorption from the helium cluster or sufficient evaporation of helium atoms, which in turn produces an attenuation of the beam.

III. Results

A. Na_2: Triplet-to-Triplet Transitions. Using a Ti:Al_2O_3 and a dye laser (DCM dye) combined with LIF detection, we have observed the $1^3\Sigma_g^+ \leftarrow 1^3\Sigma_u^+$ transition of Na_2 formed on the surface of a helium cluster (Figure 3). The LIF spectrum consists mainly of a progression of vibrational bands originating from the $v'' = 0$ state of the dimer. While it could be expected that effectively all dimers will cool to the lowest vibrational level in the time span between pick-up and laser excitation, we have found that a small proportion of clusters in the beam are doped with sodium dimers in the $v'' = 1$ state. This indicates that the cooling of vibrationally excited lower $1^3\Sigma_u^+$ electronic state dimers is relatively slow (tens of microseconds), while the vibrational cooling of electronically excited dimers (see below) occurs on the scale of several nanoseconds. The vibrational progression resulting from transitions arising from $v'' = 1$ is also shown in Figure 3.

Vibrational numbering of the observed bands is accomplished by direct comparison of the band positions with the work of Färbert et al.[14] A cluster-induced shift of one or more vibrational spacings can be ruled out by comparing the $\Delta G(v)$ of both the gas-phase and helium cluster data. Each vibrational band is broadened to the high-frequency side due to interaction with the helium cluster. Each peak has a full width at half-

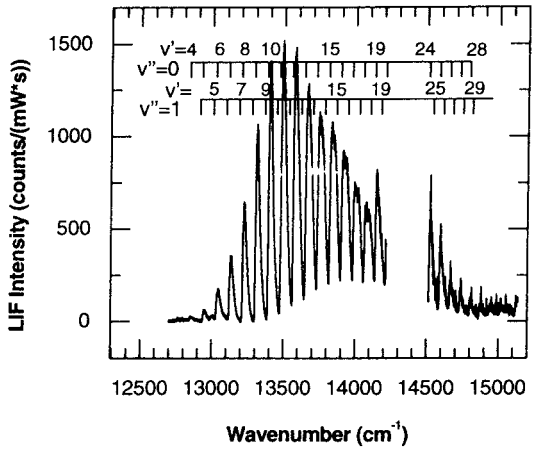

Figure 3. LIF excitation spectrum of the $1^3\Sigma_g^+ \leftarrow 1^3\Sigma_u^+$ transitions of Na_2 on the surface of a helium cluster displaying the transitions from both $v'' = 0$ and $v'' = 1$ to the $v' = 4-29$ levels. The gap in the spectrum is the result of a frequency region that could not be obtained with the lasers employed in the experiment.

TABLE 1: Comparison of the Vibrational Band Positions ($(v', v'' = 0)$ in cm^{-1}) of the $1^3\Sigma_g^+ \leftarrow 1^3\Sigma_u^+$ Transition of Na_2 between the Gas-Phase Work of Färbert and This Work, Where the Dimer Is Formed on the Surface of a Helium Cluster (Shifts Are Given in Column 4)

v'	Färbert et al.	this work	shift
4		12 841.0	
5		12 927.2	
6		13 023.0	
7		13 114.0	
8	13 196.0	13 202.8	6.8
9	13 286.4	13 292.7	6.3
10	13 376.1	13 380.8	4.7
11	13 464.9	13 468.6	3.7
12	13 551.5	13 555.8	4.3
13	13 637.7	13 643.3	5.6
14	13 721.4	13 727.3	5.9
15	13 806.3	13 812.7	6.4
16	13 887.7	13 894.5	6.8
17	13 969.2	13 974.7	5.5
18	14 049.5	14 053.7	4.2
19	14 127.8	14 133.6	5.8
20	14 206.5	14 211.4	4.9
21	14 283.5		
22	14 360.5		
23	14 435.3		
24	14 508.5	14 513.3	4.8
25	14 580.9	14 584.7	3.8
26	14 652.0	14 656.2	4.2
27	14 722.0	14 725.6	3.6
28	14 790.9	14 794.9	4.0
29	14 858.7	14 862.4	3.7

maximum (fwhm) of approximately 30 cm^{-1}, which was found to be independent of the helium cluster size in the range probed in this experiment, which corresponds to average cluster sizes of 1000−8000 atoms per cluster. A listing of the vibrational band positions is given in Table 1. Since successive vibrational bands overlap due to the broadening introduced by the helium cluster, the origin of each transition was determined by deconvoluting adjacent bands. The phonon side band which extends to higher frequencies on each band was empirically fit to a modified Gaussian line-shape function and subtracted from the band of the next higher vibrational level. This method provides a true baseline from which an accurate measure of the wavenumber of the band origin can be derived. The comparison to the gas-phase study[14] establishes that the overall shift due to the interaction with the helium cluster is 5 ± 1 cm^{-1}.

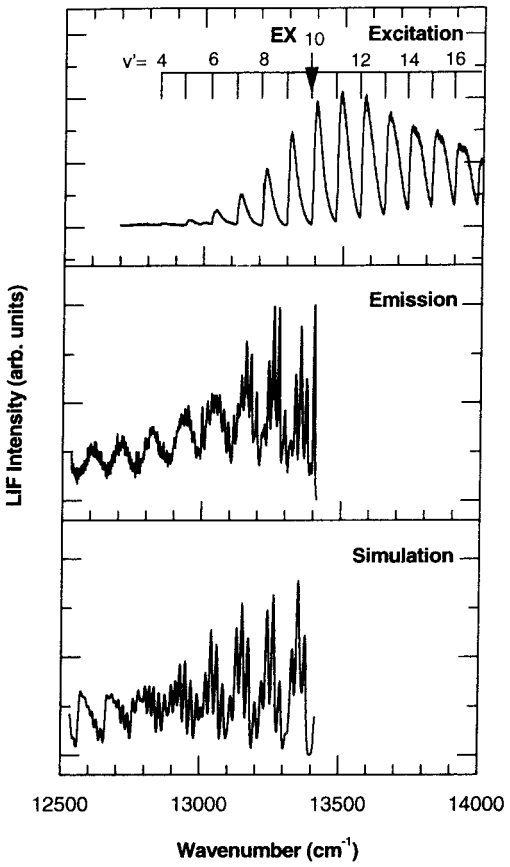

Figure 4. Emission spectrum of one of the $1^3\Sigma_g^+ \rightarrow 1^3\Sigma_u^+$ transitions of Na_2 (middle panel). The emission spectrum was obtained by exciting the $v' = 10$ vibrational level at the point marked EX (upper panel). The model spectrum (lower panel) was obtained from the calculated transitions using the RKR potential curves convoluted with a Gaussian line-shape function while fitting the level populations. The excitation line was not included in the simulation.

Information on the lowest triplet state of Na_2 can be obtained by recording the emission spectrum resulting from the excitation of the $1^3\Sigma_g^+ \leftarrow 1^3\Sigma_u^+$ transition. Figure 4 displays the emission spectra corresponding to the excitation of the $v' = 10$ vibrational level in the $1^3\Sigma_g^+$ state. The emission lines can be assigned by modeling the spectrum using the Rydberg−Klein−Rees (RKR) potential energy curves for both the upper and lower states.[11,33] An RKR potential energy curve of the excited state was obtained using the molecular constants obtained from ref 14 using a standard algorithm[34] that integrates the RKR equations by Gaussian quadrature. The calculated emission spectrum shown in Figure 4 is produced by convoluting the gas-phase line positions calculated using the RKR potential curves with a Gaussian line-shape function of 7 cm^{-1} width that approximately corresponds to the resolution of the monochromator used in obtaining the emission spectrum. The narrow line width implies that emission is arising from dimers in the gas phase that have desorbed from the helium cluster surface as a consequence of the vibrational relaxation. A least-squares fit of the intensities of the calculated levels to the observed spectrum yields the relative populations that are displayed in Figure 5. The high signal-to-noise level of the experiment allowed observation of fluorescence originating from $v' = 10$ down to $v' = 0$. The emission spectrum displays clearly that emission back to the lowest triplet state is obtained from all vibrational levels in the (c)$1^3\Sigma_g^+$ manifold up to the level that is excited by the laser. This can be attributed to vibrational energy relaxation of the electronically excited molecule due to its proximity with the

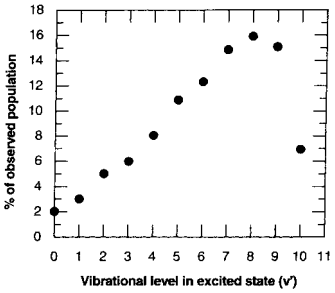

Figure 5. Populations of the excited vibrational levels in the $1^3\Sigma_g^+$ state of Na_2 obtained by fitting the data shown in figure 4.

host helium cluster. Within the fluorescence lifetime of the excited state (which we have calculated to be 10.9 ns using the transition dipole moment function calculated by Konowalow and co-workers[35]), energy is transferred to the cold helium cluster, leading to population of vibrational levels below the excited level followed by desorption of the dimer from the helium cluster surface. The data of Figure 5 are not consistent with a simple cascade model where single vibrational quanta are transferred sequentially to the helium cluster. We are currently undertaking experiments to directly measure with state selectivity the vibrational cooling rates by using picosecond laser pulses to prepare the excited state, followed by time-correlated photon-counting measurements of the emitted fluorescence.

B. Na_2: Modeling of the Triplet State Potential Surface. Since the perturbation induced by the helium cluster on the electronic spectrum of the alkali dimers is weak, the spectroscopic data obtained can be directly used to test the accuracy of potential energy curves calculated for the excited state. We used the Hartree−Fock damped dispersion (HFD) form proposed by Douketis et al.[36] to model the excited-state potential energy curves. The total interaction energy between the two atoms ($V_2(r)$) is split into a contribution calculated at the Hartree−Fock self-consistent-field level (ΔE^{SCF}) and a damped multipole expansion that accounts for dispersion interactions (ΔE^{CORR}).

$$V_2(r) = \Delta E^{SCF}(r) + \Delta E^{CORR}(r) \quad (1)$$

$$\Delta E^{SCF}(r) = A_1 r^{\alpha_1} e^{-\beta_1 r} + A_2 r^{\alpha_2} e^{-\beta_2 r} \quad (2)$$

$$\Delta E^{CORR}(r) = -[\sum_n C_n r^{-n} g_n(\rho r)] f(\rho r) \quad (3)$$

$$n = 3, 6, 8, 10,... \quad (4)$$

$$g_n(\rho_r) = \left[1 - \exp\left(-\frac{2.1\rho r}{n} - \frac{0.109\rho^2 r^2}{\sqrt{n}}\right)\right]^n \quad (5)$$

$$f(\rho r) = 1 - (\rho r)^{1.68} e^{-0.78\rho r} \quad (6)$$

$$\rho = \left(\frac{IP}{13.6\ eV}\right)^{0.66} \quad (7)$$

$$\rho_{12} = \frac{2\rho_1\rho_2}{\rho_1 + \rho_2} \quad (8)$$

The universal damping functions f and g scale with ρ, which is determined by the ionization potentials of the two interacting atoms.

We confirmed the validity of the HFD ansatz for the description of the lowest triplet state ($(a)1^3\Sigma_u^+$) of the alkali dimers by applying the above set of equations to Na_2 after obtaining the HF-SCF energy using the GAUSSIAN 92 suite of programs and adopting the long-range C_n coefficients calculated by Marinescu and Dalgarno.[37] The parameters of the potential are listed in Table 2. As expected, the HFD potential reproduces the experimentally observed vibrational levels of the $(a)1^3\Sigma_u^+$ state[11,30] within 3 cm^{-1}. The bound states were calculated using the program LEVEL 6.0 provided by R. J. LeRoy.[38]

TABLE 2: Parameters of the Hartree−Fock Damped Dispersion (HFD) Potential for the $(a)1^3\Sigma_u^+$ State of Na_2[a]

parameter	value	parameter	value
A_1	1.010×10^6	β_2	1.7861
α_1	5.7348	C_6	7.0789×10^6
β_1	4.3736	C_8	5.3813×10^8
A_2	9.6005×10^4	C_{10}	5.3236×10^{10}
α_2	1.7342	ρ	0.5261

[a] The HF-SCF energy was obtained using the GAUSSIAN 92 suite of programs, and the long-range coefficients were taken from the work of Marinescu and Dalgarno.[37] Values given for R in angstroms and $V(R)$ in cm^{-1}.

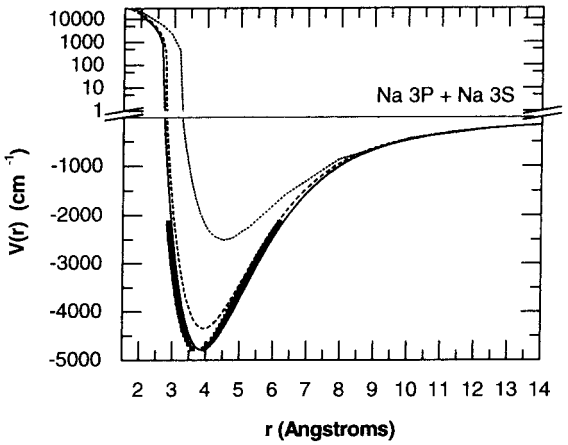

Figure 6. Potential energy curves of the excited $1^3\Sigma_g^+$ state of Na_2. Comparison of the HFD semiempirical form (solid line) to the RKR turning points (solid squares) derived from the data of Färbert et al.[14] The dotted line is the SCF calculation that includes resonant exchange interaction but no induction effects. The dashed line is the full SCF including polarization. The zero of energy has been referenced to the Na (3S) + Na (3P) asymptote.

It is of course interesting to test the validity of extending the HFD hypothesis from a state like $1^3\Sigma_u^+$, where overlap repulsion, dispersion attraction, polarization, and penetration effects account for the whole interaction, to a state like $1^3\Sigma_g^+$ ($\sigma_g(ns)\sigma_g(np)$), where resonant exchange interaction leads to a much larger binding energy. There is, however, a well-known problem with proper dissociation of some electronic states within the SCF method. Indeed, proper dissociation of the $1^3\Sigma_g^+$ state requires a two-configuration wave function within the method of molecular orbitals. Two forms of molecular wave functions have been used for the $1^3\Sigma_g^+$ state of Na_2. In the first approach, shown with a dotted line in Figure 6, only coefficients for the $\sigma_g\sigma_g$ and $\sigma_u\sigma_u$ configurations were determined variationally for different R's, whereas molecular orbitals were always given as linear combinations of orbitals of free atoms. This approach allows the inclusion of the long-range C_3/R^3 interaction in addition to the valence repulsion and penetration effects. In the second approach, shown with a dashed line in Figure 6 and listed in Table 3, we also allowed for variational optimization of molecular orbitals, thus including polarization (induction) terms. Given the large quadrupole moment associated with the excited-state p orbital, these terms represent a significant fraction

TABLE 3: Hartree−Fock Self-Consistent-Field (HF-SCF) Energy Calculated for the (c)$1^3\Sigma_g^+$ State of Na_2 Including Both Resonant Exchange and Induction Effects. Coefficients for the $\sigma_g\sigma_g$ and $\sigma_u\sigma_u$ Configurations Were Determined Variationally for Different R's, and the Calculation Allowed for Variational Optimization of Molecular Orbitals, Thus Including Polarization (Induction) Terms

R (angstroms)	$V(r)$ (cm^{-1})	R (angstroms)	$V(r)$ (cm^{-1})
1.85	21 069.83	4.13	-4301.47
2.12	11 972.59	4.23	-4241.25
2.38	5837.56	4.50	-4016.13
2.65	1608.46	4.76	-3726.53
2.91	-1166.82	5.29	-3084.41
3.17	-2865.59	6.35	-1951.53
3.28	-3318.04	7.94	-965.39
3.39	-3667.67	10.05	-450.55
3.49	-3929.71	12.70	-216.55
3.60	-4117.52	15.87	-108.36
3.70	-4242.77	19.57	-56.15
3.81	-4315.58	23.81	-29.83
3.91	-4344.74	31.74	-10.84
4.02	-4337.85	52.90	0.00

TABLE 4: Parameters of the Hartree-Fock Damped Dispersion (HFD) Potential for the (c)$1^3\Sigma_g^+$ State of Na_2[a]

parameter	value (au)	parameter	value (au)
ρ	0.405	C_6	4094
C_3	12.26	C_8	4.445×10^4

[a] The long-range coefficients were taken from the work of Marinescu and Dalgarno.[37]

of the binding energy and are responsible for a sizable contraction of R_e.

Since the $1^3\Sigma_g^+$ excited state correlates to the Na(3S) + Na(3P) separated atomic limit, the dispersion interaction does not involve two spherically symmetric atoms. The parameter ρ of the HFD potential, which determines the magnitude of the damping of the dispersion interaction at short internuclear distances, is a measure of the spatial extent of the exponentially decreasing tail of the electronic wave function and has been obtained assuming as a model the interaction between two ground-state (spherical) hydrogen atoms in their lowest triplet state.[36] Therefore, for ground-state atoms, ρ scales with the ionization potentials of the individual atoms. When one of the two atoms is in an excited state, the spherical symmetry of the atomic fragments is broken and the correlation with the ionization potential may not be generally applicable anymore. Therefore we decided to hold ρ as an adjustable parameter in the calculation. The fitting process was aided by using the spectroscopic constants determined by Färbert and co-workers[33] to produce an RKR potential curve of the $1^3\Sigma_g^+$ state. The C_6 and C_8 coefficients of Marinescu and Dalgarno[37] were used in the calculation. The C_8 coefficient of ref 37 contains both induction and dispersion terms. Since the HF-SCF energy that we have calculated includes the induction energy, we needed to separate the two contributions to the calculated C_8. Using the calculated value of the static quadrupole moment of the 3P state and the polarizability of the 3S Na, we calculated the induction contribution and subtracted this from the C_8 coefficient to obtain the dispersion contribution. The value we obtain is reported in Table 4. Using these dispersion coefficients, the optimum value of ρ was found to be 0.405, which brings the HFD potential energy curve into agreement with the RKR data. The value of ρ obtained from the fitting procedure for the $1^3\Sigma_g^+$ state (0.405) is less than that calculated for the $1^3\Sigma_u^+$ state (0.5261, calculated from the ionization potential of ground state Na atoms) and therefore provides more damping of the long-range attraction than that found in the lowest triplet state of Na_2. The separated atom limit of the excited $1^3\Sigma_g^+$ state corresponds to a spherical 3s orbital on one Na atom and a 3p orbital on the other Na atom aligned parallel to the internuclear axis. Since the spatial extent of the 3p orbital is larger than the 3s, the ground-state Na begins to feel the overlap repulsion with the p orbital sooner as the internuclear distance is decreased, and therefore greater damping of the dispersion energy is required than that found between two 3s Na atoms. Instead of fitting ρ one can use eq 7, in which, according to the original ansatz, the ionization potentials of a 3^2S(Na) and a 3^2P-(Na) state are combined linearly. This calculation yields a value of $\rho = 0.4358$. Using this value of ρ, the HFD potential energy curve that results is 150 cm^{-1} (or 3%) deeper at r_e and the outer turning points are approximately 0.15 Å too large. The optimum value of ρ that results from fitting to the RKR data (0.405) produces even more damping of the long-range attraction than that obtained with the ionization potential of the excited state (0.4358). Since the contribution to the dispersion is, in this case, not the dominant one, a reasonably accurate result is achieved even with an imperfect knowledge of the parameter ρ. The details of the extension of the HFD ansatz to excited molecular states with an assessment of its predictive ability will be discussed in a forthcoming publication.[39]

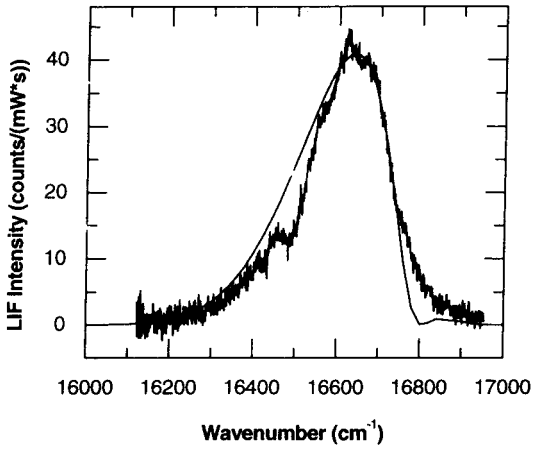

Figure 7. LIF excitation spectrum of the $1^3\Pi_g \leftarrow 1^3\Sigma_u^+$ transition of Li_2 on the surface of a helium cluster compared to the spectrum calculated using the excited-state potential energy curve of Konowalow.[42]

The maximum of the Franck−Condon distribution of the calculated spectrum using the RKR curve occurs at $v' = 15$, while the observed spectrum for the $1^3\Sigma_g^+ \leftarrow 1^3\Sigma_u^+$ transition on helium clusters yields a maximum at $v' = 11$. The HFD potential predicts a maximum at $v' = 12$. This is due to the presence of vibrational hot bands arising from transitions out of $v'' = 1$ in the lower state that distort the band intensities and do not allow a simple estimation of the absorption strength by comparing the peak heights of the various bands in the spectrum.

C. Bound−Free Transitions for Triplet Li_2 and K_2. In contrast to the structured bound−bound transitions such as those observed for Na_2, excitation from the lowest triplet state of the alkali dimers to a repulsive excited electronic state will give rise to a diffuse band devoid of vibrational structure. The repulsive $1^3\Pi_g$ electronic states of both Li_2 and K_2 have been observed by initial preparation of the triplet dimer on the surface of the helium clusters. Figure 7 displays the excitation spectrum of the $1^3\Pi_g \leftarrow 1^3\Sigma_u^+$ transition of Li_2 as observed in our apparatus. The band appears approximately 800 cm^{-1} to the blue of the atomic Li $2^2P_{3/2,1/2} \leftarrow {}^2S_{1/2}$ transition. This transition was previously observed in a heat pipe containing 0.11 atm of Li vapor at 1346 K.[40] At this gas density, the Li atomic

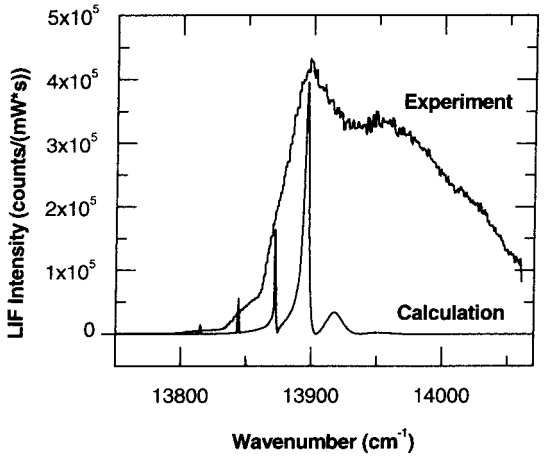

Figure 8. LIF excitation spectrum of the $1^3\Pi_g \leftarrow 1^3\Sigma_u^+$ transition of K_2 on the surface of a helium cluster compared to the spectrum calculated using the excited-state potential energy curve of Magnier.[48]

transition was broadened to 100 nm. The Li_2 $1^3\Pi_g \leftarrow 1^3\Sigma_u^+$ transition appeared as a small shoulder on the blue wing of the atomic transition. In our experiment, the Li_2 $1^3\Sigma_u^+$ state is formed on the cold helium cluster where only the lowest ($v'' = 0$) vibrational state appears to have significant population (see below).

The profile of the absorption band can be modeled quantum mechanically using the potential energy surfaces of the upper and lower states. The program BCONT 1.4, written by R. J. Leroy, was used for the calculation.[41] The nuclear wave functions were determined using Numerov−Cooley integration, and the Franck−Condon overlap integrals between the upper and lower states were calculated. The ab initio potential energy curves for the excited state calculated by both Konowalow et al.[42] and Schmidt-Mink et al.[1] along with the RKR potential of the lower state[43] were used to model the transition. The results of the calculation for a transition originating from $v'' = 0$ are displayed in Figure 7. A Boltzmann distribution with a temperature of 0.4 K was used to determine the J populations. Due to their similarity, the two ab initio potentials give almost identical predictions for the experimental spectrum.

None of the features present in the experimental spectrum are attributable to absorption out of the $v'' = 1$ level, which is consistent with a triplet Li dimer that is in equilibrium with the local environment of the helium cluster. Why all Li_2 dimers are found to be in $v'' = 0$ while a reasonable fraction of the Na_2 dimers of the previous experiments were found to be in $v'' = 1$ is not clear at this point. There are several aspects of the pick-up process such as the temperature re-equilibration time that would require, and perhaps deserve, further study. Given the good sensitivity of the experimental observables to the potential, the agreement between the experiment and calculation in this case reveals the general validity of the potential energy curves of refs 1 and 42 but leaves room for some improvements.

An excitation spectrum of K-doped helium clusters in the short-wavelength region of the Ti:Al_2O_3 laser reveals a broad absorption band approximately 900 cm^{-1} to the blue of the potassium atomic lines. This is the analogous band as observed in Li_2 and can be attributed to an electronic transition originating from the $1^3\Sigma_u^+$ state of K_2 to the excited $1^3\Pi_g$ state.[44−47] Whereas Konowalow's theoretical potential[42] for the lithium dimer predicts a purely repulsive upper state, the potential energy curve calculated by both S. Magnier[48] and Jeung et al.[49] for K_2 displays an attractive well at short internuclear separations. Figure 8 displays the experimental spectrum with the profile

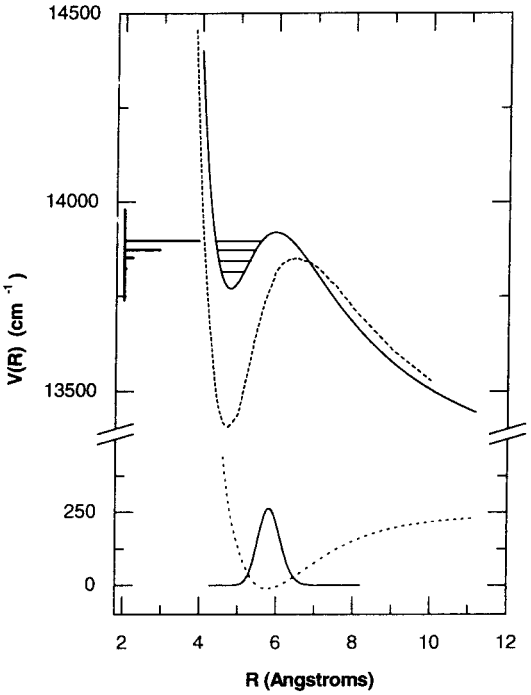

Figure 9. Potential energy diagram for the electronic states involved in the $1^3\Pi_g \leftarrow 1^3\Sigma_u^+$ transition of K_2. The positions of the experimental peak positions obtained from the K_2 molecule residing on the helium cluster are displayed as vertical bars on the y-axis. The lower state is the RKR potential curve of ref 50 and has been shifted by +243 cm^{-1} along with the excited state to make the $v'' = 0$ level coincide with the zero of the energy. The wave function for the $v'' = 0$ level is displayed. The theoretical excited-state potentials of Magnier[48] (solid line) and of Jeung et al.[49] (dashed line) are displayed. For the potential of Magnier the position of the first four quasi-bound states in the $J = 0$ excited-state potential is also shown.

calculated utilizing the same method as was used for the Li_2 $1^3\Pi_g \leftarrow 1^3\Sigma_u^+$ transition. The calculated intensities using Magnier's excited-state potential energy curve[48] and the RKR curve for the (a) $1^3\Sigma_u^+$ lowest triplet state[50] do not fit the overall profile of the absorption band. The calculation reveals bound−bound transitions at 13 815, 13 844, 13 872, and 13 896 cm^{-1} that result from overlap of the lower state wave function with the metastable levels of the excited-state potential well. A small absorption centered at 13 918 cm^{-1} is calculated due to overlap with a $J > 0$ state above the $J = 0$ barrier to the excited-state potential well. The calculated width of the bound to quasi-bound resonances increases at higher energy due to the shorter lifetime of the excited states (see Figure 9). The (incompletely resolved) peaks in the experimental spectrum occur at 13 823, 13 852, 13 873, and 13 897 cm^{-1}. These experimental values have been obtained by fitting the experimental data with Gaussian line shapes. The experimental intensity peaks at the same position as that of the calculation. A schematic of the potential energy curves and LIF excitation spectrum is diplayed in Figure 9. The RKR potential for the $1^3\Sigma_u^+$ lowest triplet state is displayed along with the wave function for the $v'' = 0$ level. The potential well in the excited state that has been calculated by Jeung et al.[49] is much too deep since it would predict the presence of 11 bound−bound transitions that would occur below 13 500 cm^{-1} that are not observed in our experimental spectrum. The potential calculated by Magnier[48] appears to possess the correct well depth in the excited state since it predicts the correct number and position of the bound levels. However, the experimental spectrum shows a significant broadening for each peak associated with a bound−bound transition and a broad fluorescence above 13 940 cm^{-1} that may

be due to the influence of the helium cluster. As we will show in the section on nonadiabatic effects, the presence of the helium cluster can induce intersystem crossings in the excited state that may significantly alter its lifetime and the resulting excitation spectrum. Also, a phonon wing could account for the broadening that extends to the blue of the bound−free spectrum.

D. Heteronuclear Alkali Dimers: NaK. Helium cluster isolation can be used for the production of heteronuclear dimers by simply adding additional pick-up cells. In contrast to the case where the mixed dimers are formed by coexpansion from the same nozzle, each pick-up cell can be kept at a different temperature as required by the different vapor pressure of the substances to be mixed. We have performed experiments using two collinear pick-up cells to dope the cluster beam with mixed alkali metal dimers. In the configuration used for these experiments, the helium cluster beam encounters a pick-up cell containing Na vapor immediately after emerging from the skimmer. After emerging from this pick-up cell, 3 mm downstream another cell is encountered, where an equal density of potassium vapor is maintained. If, for example, a sodium pressure is maintained in the first cell such that 30% of the clusters pick up a sodium atom (and therefore 9% pick up two sodium atoms) with an equal pressure of potassium in the second cell, an approximately equal number of mixed and homonuclear dimers will be present on the helium clusters after emerging from the second cell.

Group IA and IIA metals will preferentially form singlet homonuclear dimers over the heteronuclear species due to the stronger bond in the former species. Helium cluster isolation can provide direct access to the triplet manifold of NaK, with little interference from the singlet electronic transitions, due to the selectivity of the method for the triplet states. Since for heterodimers there is no longer a parity selection rule governing the electronic transitions, more excited states are available for spectroscopic investigation. Using LIF detection, we have observed two electronic transitions in NaK: the (c)$2^3\Sigma^+ \leftarrow$ (a)$1^3\Sigma^+$ and the (d)$2^3\Pi \leftarrow$ (a)$1^3\Sigma^+$. The spectra can be seen in Figure 10 and 11. Similar to the case of Li_2 and in contrast to that of Na_2 described above, in both spectra only features originating from $v'' = 0$ of the lowest triplet state have been detected.

The (c)$2^3\Sigma^+ \leftarrow$ (a)$1^3\Sigma^+$ transition of NaK has been previously studied by Kowalczyk and Sadeghi[51] using perturbation-facilitated spectroscopy. They were able to produce a nonstandard RKR potential energy curve using data from $v' = 20$ to 40 which were extrapolated to $v' = 0$ (unlike a normal RKR potential, where data from $v' = 0$ to 40 would be used). They were able to unambiguously assign vibrational quantum numbers to the observed levels. Since $v' = 20$ is the first vibrational level above $v = 0$ in the (B)$1^1\Pi$ state which perturbs the (c)-$2^3\Sigma^+$ state, the vibrational states with $v' < 20$ could not be accessed. The bands observed in our excitation spectrum can be assigned using the numbering proposed by ref 51. It can be seen from Figure 10 that our experiment probes the $v' = 6-18$ levels of the transition around the peak of the Franck−Condon distribution from the $v'' = 0$ level in the lowest triplet state. Therefore, our data are complementary to those described in ref 51. The excitation spectrum calculated using the RKR potential curve of ref 51 for the (c)$2^3\Sigma^+$ state and that of ref 9 for the (a)$1^3\Sigma^+$ is also displayed in Figure 10 as thick solid bars. This calculation assumed a constant transition dipole moment $\mu(R)$. It can be seen that the calculated level spacing is not in exact agreement with the experiment, which can be expected since the extrapolation of the data in ref 51 may not be valid all the way to vibrational levels at the bottom of the potential well. In particular, the ω_e that is predicted by the RKR potential curve must be increased to agree with the experimental line positions of the $v' = 6-17$ levels. This would correspond to a potential energy curve that is narrower around the region of the minimum.

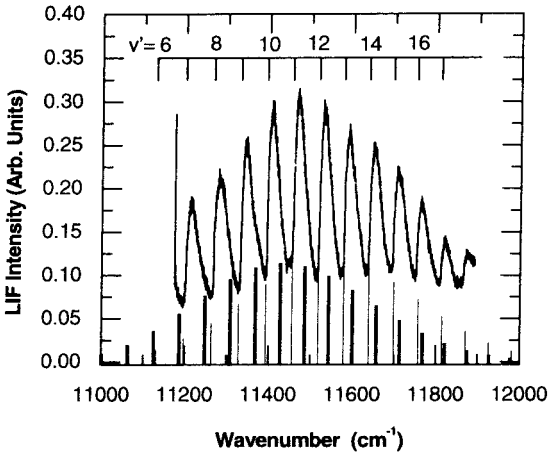

Figure 10. Excitation spectrum of the (c)$2^3\Sigma^+ \leftarrow$ (a)$1^3\Sigma^+$ transition of NaK. Thick bars are the calculated spectrum using the RKR curve of Kowalczyk et al.[51] Thin bars are calculated using the theoretical potential energy curve of Stevens et al.[52]

TABLE 5: Comparison of the Vibrational Band Positions (in cm^{-1}) of the (c)$2^3\Sigma^+ \leftarrow$ (a)$1^3\Sigma^+$ Transition of NaK[a]

v' upper	this work	Kowalczyk et al. RKR potential	Stevens et al. calculated potential
6	11 130.8	11 184.5	11 130.8
7	11 200.1	11 245.4	11 197.9
8	11 267.6	11 306.0	11 264.0
9	11 331.8	11 366.3	11 329.2
10	11 394.6	11 426.2	11 393.4
11	11 456.4	11 485.8	11 456.6
12	11 518.8	11 545.1	11 518.9
13	11 579.0	11 604.1	11 580.0
14	11 638.7	11 662.8	11 640.0
15	11 696.5	11 721.1	11 699.7
16	11 753.2	11 779.1	11 758.0
17	11 810.6	11 836.8	11 815.3
18	11 865.6	11 894.1	11 871.6

[a] The T_e for the potential of Stevens et al. was increased by 310.3 cm^{-1} to bring the lowest observable level ($v' = 6$) into agreement with the calculated levels. The RKR potential of ref 51 for the (c)$2^3\Sigma^+$ state of NaK was used in the calculation of the vibrational band positions.

The calculations for the various vibrational levels using the theoretically derived potential of Stevens et al.[52] for the (c)-$2^3\Sigma^+$ state are also displayed in Figure 10 as thin bars. The theoretical potential curves of Stevens *et al.* were calculated using full configuration interaction (CI), employing effective core potentials. The T_e value of the theoretical potential needs to be increased by approximately 310 cm^{-1} to bring the $v' = 6$ level into agreement with our experimental data derived from the helium cluster isolation technique. However, when that is done, the shape of the potential accounts reasonably well for the measured vibrational spacings. Table 5 gives a complete listing of our measured line positions and the comparison with those derived from the theoretical and RKR potential energy curves. The intensity distribution given by the Franck−Condon factors calculated for both potentials displays reasonable agreement with our experimental data for the dimer on the surface of a helium cluster.

The (d)$2^3\Pi \leftarrow$ (a)$1^3\Sigma^+$ transition of NaK as observed on the helium cluster lies in a slightly more congested region of the spectrum than that of (c)$2^3\Sigma^+ \leftarrow$ (a)$1^3\Sigma^+$. At the low-frequency

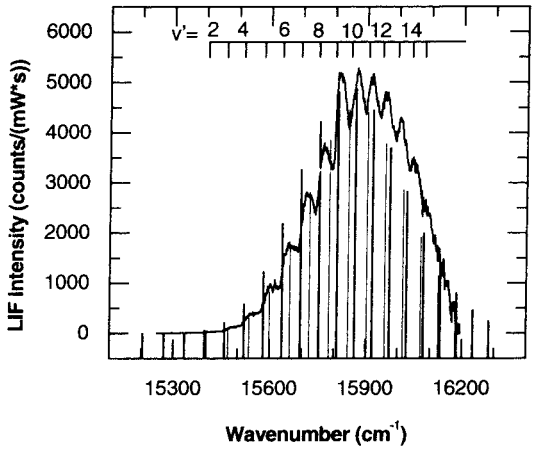

Figure 11. Excitation spectrum of the (d)$2^3\Pi \leftarrow$ (a)$1^3\Sigma^+$ transition of NaK. Thick bars are the calculated transitions using the RKR potential energy curve of Kowalczyk,[55] while thin bars mark the transitions calculated using the theoretical potential of Stevens et al.[52]

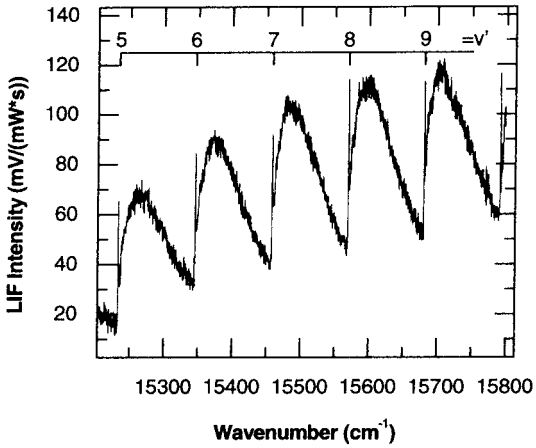

Figure 12. LIF excitation spectrum of the $1^1\Sigma_u^+ \leftarrow 1^1\Sigma_g^+$ transition of Na_2 displaying the transitions to $v' = 5-9$. A sharp zero phonon line can be seen at the origin of each vibrational band.

end of the excitation spectrum, the $1^3\Sigma_g^+ \leftarrow 1^3\Sigma_u^+$ transition of Na_2 begins to appear. At the high-frequency end, above 15 800 cm^{-1}, a strong quartet transition of Na_3 begins to appear. If the vapor pressure of Na in the first pick-up cell is carefully controlled, the fluorescence resulting from the NaK transition can dominate in the region of the Na_3 trimer transition and the spectrum can be extended to include the entire envelope of the Franck−Condon distribution.

Whereas the (c)$2^3\Sigma^+$ state of NaK correlates to the K(4P) + Na(3S) atomic limit, the (d)$2^3\Pi$ state correlates to the Na(3P) + K(4S) limit. The presence of this state has been known for over 60 years[53] and has been studied quite extensively since it directly perturbs the (D)$1^1\Pi$ state[54,55] of NaK. Kowalczyk[55] was able to observe the (d)$2^3\Pi$ state through the (d)$2^3\Pi \leftarrow$ (X)$^1\Sigma^+$ intercombination transition. A definitive vibrational assignment could be made by observing the isotope shifts of the vibrational bands. The $J = 0$ spectrum calculated from the RKR potential energy curve given in ref 55 is displayed in Figure 11 as thin bars along with the spectrum obtained of the molecule formed on the surface of the helium cluster. The spectrum calculated using the theoretical potential energy curve of Stevens et al. is shown for comparison as thick bars. The potential energy curve of ref 9 for the lowest triplet state of NaK was used in both calculations. It can be seen that the overall intensity envelope is in good agreement with the observed transition. A direct comparison of the band positions of the spectrum of the NaK molecule on the helium cluster with the gas-phase work cannot be made since the broadening due to the presence of the cluster causes overlap between successive vibrational bands. On the other hand, it is quite clear that both theoretical potentials are not entirely adequate to describe the experimental results. Overall, the transitions in the (2,0) to (15,0) range (where the notation (v',v'') is used) are clearly resolved in the spectrum. Above 16 100 cm^{-1}, the lines appear to merge and complete resolution is not possible. The observation of these transitions in NaK provides a clear demonstration of the helium cluster isolation technique in the study of van der Waals molecules formed from the addition of two distinctly separate species to the helium cluster.

E. Na_2: Singlet-to-Singlet Transitions. Although a greater quantity of helium clusters becomes doped with triplet sodium dimers, the presence of the singlet species can be detected through the observation of the $1^1\Sigma_u^+ \leftarrow 1^1\Sigma_g^+$ transition of Na_2 if the Na vapor pressure in the pick-up cell is increased by an order of magnitude. This is the well-known A ← X system of the sodium dimer, and its observation on the helium cluster was first reported in ref 18. The excitation spectrum of the $v' = 5-9$ bands is displayed in Figure 12. The structure observed for each vibrational band differs significantly from that observed for each of the triplet transitions and resembles the structure typical of matrix-isolated species. Each band possesses a sharp zero phonon line of about 0.8 cm^{-1} width which corresponds to the pure electronic transition of the Na_2, followed by a phonon wing extending to higher frequencies than the zero phonon line. High-resolution spectroscopy of these bands[18] has revealed that the zero phonon line is red-shifted by only 2.8 cm^{-1} relative to the band origin of the rotational structure of the gas-phase dimer. Figure 13 displays a high-resolution spectrum of the zero phonon region of the $v' = 9$ vibrational band. A strikingly similar spectrum was found for glyoxal inside helium clusters[21] by Hartmann et al., who successfully modeled the spectrum on the basis of the dispersion curve for He II. The peaks in the glyoxal spectrum that are blue-shifted by 5.4 and 10.5 cm^{-1} with respect to the zero phonon line were attributed to the coupling to the larger density of states corresponding to the roton and maxon extrema in the energy vs momentum dispersion curve measured for liquid helium by means of neutron scattering. The spectrum of Figure 13 consists of three peaks at higher energy than the zero phonon line superimposed on the broad background of the phonon wing of the transition. The second and third peaks are assigned to the roton and maxon peaks since they occur at the same energy relative to the zero phonon line in both glyoxal and Na_2. The first peak remains unassigned, although it occurs at the same frequency relative to the zero-phonon line as that assigned to rotational excitation of the glyoxal inside the helium cluster. Due to the different rotational structure of the transitions in glyoxal and Na_2, an alternative assignment for the peak in the spectrum of Na_2 must be sought. Since the sodium dimer is located on the surface of the cluster, the peak could be due to a coupling to the surface modes of the helium cluster.

The overall shape of the phonon sideband of the singlet-to-singlet transition is very sensitive to the average helium cluster size in the beam. We can easily change the average size and distribution by varying the stagnation conditions. The average cluster size is most greatly affected by changes in the nozzle temperature as opposed to stagnation pressure or nozzle diameter.[56] The width of the phonon sideband varies from 110 cm^{-1} at a nozzle temperature of 17.5 K (larger average size) to approximately 30 cm^{-1} at a temperature of 22 K (smaller average size). It is interesting to note that in the same range the position of the roton maximum does not shift appreciably.

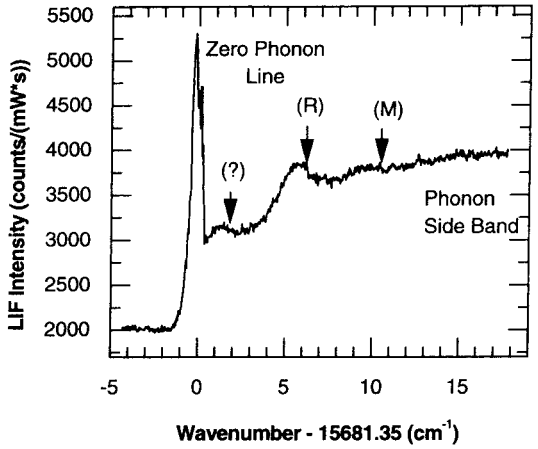

Figure 13. Expanded view of the zero phonon region of the $1^1\Sigma_u^+ \leftarrow 1^1\Sigma_g^+$ transition of Na_2. The zero of the frequency scale has been taken as the peak of the zero phonon line. The phonon sideband is clearly visible as a broad absorption to the blue of the zero phonon line. The peak labeled (R) corresponds to the energy of the roton maxima in the dispersion curve of liquid helium. The peak labeled (M) occurs at the maxon energy. The peak labeled (?) has not been definitively interpreted at this point.

It is also interesting that in the triplet spectra the zero phonon lines are absent and the broadening of each vibrational band is smaller (30 cm^{-1} for triplets vs 110 cm^{-1} for singlets, both measured at a nozzle temperature of 17.5 K). In accordance with the spectroscopy of matrix-isolated species, the intensity of the zero phonon line decreases as the coupling to the matrix increases, and there is a greater inelastic transfer of energy to phonons in the matrix. The absence of a zero phonon line for the triplet transition would suggest that the coupling of the electronic energy with the helium cluster is greater in the excited triplet state of Na_2 as compared to the singlet state. On the other hand, the smaller width of the phonon wing points toward a smaller coupling in the excited triplet state.

F. Nonadiabatic Effects. In the course of our experiments to probe the alkali dimer triplet states we have encountered a number of unexpected results. In addition to the surprisingly small size of the spectral perturbations, we have observed excitation transfer processes between alkali species attached to the same helium cluster. The collinear pick-up cell technique can be used to dope the helium clusters with both Na and K. If the helium clusters become doped with both Na_2 and K, the emission spectrum of the $1^3\Sigma_g^+ \rightarrow 1^3\Sigma_u^+$ transition of Na_2 displays the presence of the K $4^2P_{3/2,1/2} \rightarrow 4^2S_{1/2}$ atomic lines. In this region of the spectrum there is no other transition of a potassium-containing species that could produce the K atomic lines. Paradoxically, a selective excitation spectrum of the $1^3\Sigma_g^+ \leftarrow 1^3\Sigma_u^+$ transition of Na_2 can be taken by scanning the frequency of the excitation laser and monitoring the fluorescence by positioning the monochromator to pass only the fluorescence from the K $4^2P_{3/2,1/2} \rightarrow 4^2S_{1/2}$ atomic lines! The resulting spectrum is diplayed in Figure 14. The (30, 0) to (35, 0) transitions of the sodium triplet dimer can be clearly seen. The K atomic resonance is at a lower energy than the molecular transitions that are being excited. This proves the presence of helium clusters in the beam that contain both triplet Na_2 and *uncomplexed* K atoms. After excitation of the triplet dimer, collisional transfer of energy must occur between the dimer and atom on the surface of the cluster. We have searched for other explanations of these observations, but we had to conclude that the above should be taken as evidence that some helium clusters can contain more than one dopant species which remain separated on the cluster surface far enough that they do not perturb the excitation spectra.

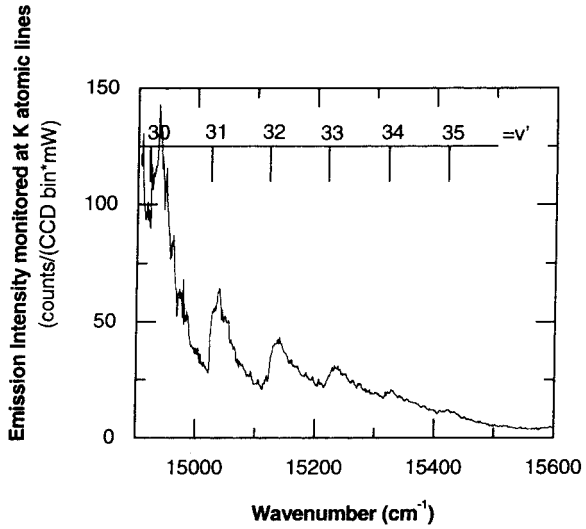

Figure 14. Selective excitation spectrum of the $1^3\Sigma_g^+ \leftarrow 1^3\Sigma_u^+$ transition of Na_2 obtained by monitoring exclusively the fluorescence around the K atomic lines with a band-pass of 50 cm^{-1}.

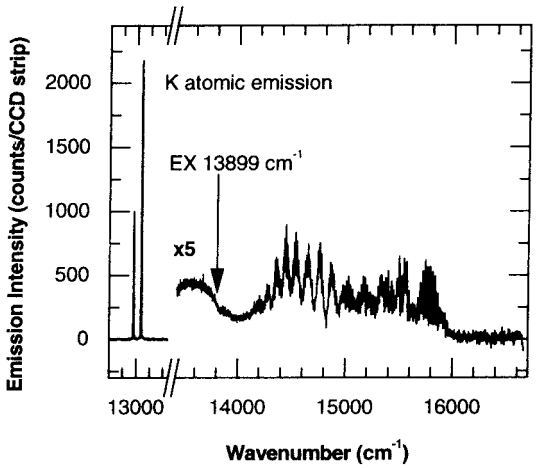

Figure 15. Emission spectrum obtained by exciting the $1^3\Pi_g \leftarrow 1^3\Sigma_u^+$ transition of K_2 at 13 895 cm^{-1}. The potassium $4^2P_{3/2,1/2} \leftarrow 4^2S_{1/2}$ atomic lines are apparent near 13 045 and 12 998 cm^{-1} resulting from the dissociation of the excited-state K_2 molecule. The B $\rightarrow$ X transition of the potassium singlet dimer is also detected to the blue of the excitation line.

We will turn now to the emission spectra obtained after excitation of K dimers. One would predict that an emission spectrum obtained by exciting the $1^3\Pi_g \leftarrow 1^3\Sigma_u^+$ dissociating transition would only reveal atomic K resonance fluorescence resulting from the dissociation of the dimer to the 4P + 4S separated atomic limit. Instead, the actual emission spectrum (see Figure 15) reveals very surprising results. In addition to the K atomic resonance fluorescence from the $4^2P_{3/2,1/2} \rightarrow 4^2S_{1/2}$ transition, fluorescence is also observed to the blue (higher energy) of the excitation position. This is the well-known (B)-$1^1\Pi_u \rightarrow (X)1^1\Sigma_g^+$ transition of K_2. It can be modeled by calculating the emission spectrum using the RKR potential curves of the ground and excited states.[57] The spectrum can be fit assuming there is population in the excited vibrational levels $v' = 0-12$. The appearance of this fluorescence reveals a phenomenon that appears to be ubiquitous in the spectroscopy of high-spin alkali clusters on the surface of helium clusters.

The observation of fluorescence at a higher energy than the exciting transition can only be associated with two processes,

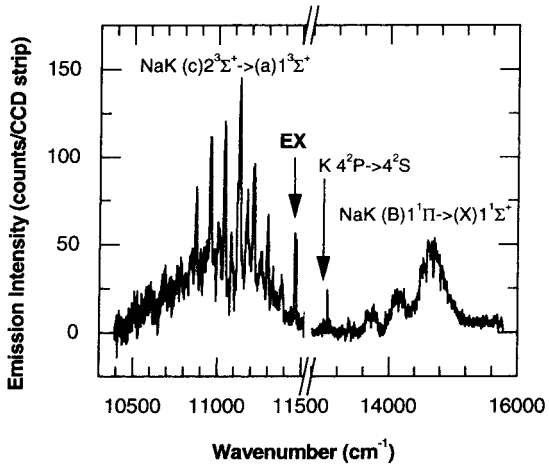

Figure 16. Emission spectrum after excitation of the (c)$2^3\Sigma^+ \leftarrow$ (a)-$1^3\Sigma^+$ transition of NaK. The excitation frequency is marked by the arrow at 11 460.9 cm^{-1}. The K atomic lines are not resolved in the spectrum.

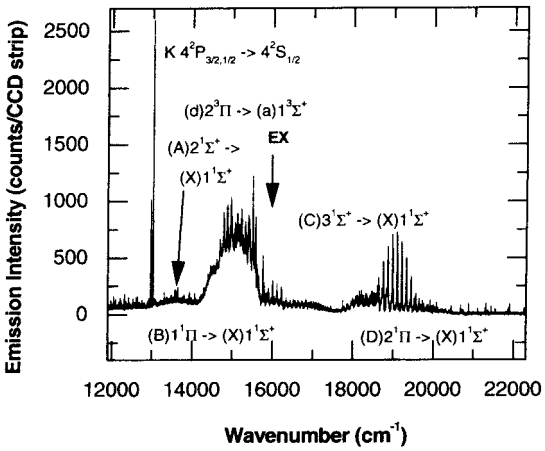

Figure 17. Emission spectrum after excitation of the (d)$2^3\Pi \leftarrow$ (a)-$1^3\Sigma^+$ transition of NaK revealing transitions from numerous singlet and triplet electronic states. The excitation frequency is marked by EX.

multiphoton excitation or conversion of potential energy into electronic energy. The presence of a multiphoton process can be ruled out since the laser power dependence of the LIF intensity of the measured dimer transitions are linear across three decades of laser power. We must conclude that intersystem crossing into the singlet manifold of dimer electronic states with subsequent fluorescence to the ground state causes the appearance of the blue-shifted fluorescence since the well depth of the covalently bound singlet state is significantly deeper than the triplet state.

The presence of blue-shifted fluorescence is more easily understood in our previous studies of quartet (three parallel spins) trimers of Na_3 and K_3 on helium clusters.[58] As in the case of the weakly bound triplet states of the dimers, the helium cluster isolation technique will favor the formation of the quartet trimers which are only bound by van der Waals forces. As we have shown in previous work,[58] laser excitation to an excited quartet state of Na_3 and K_3 is followed by a nonadiabatic spin−flip process that leads to the formation of the corresponding doublet trimer, which subsequently dissociates into an atom and a singlet dimer. This change in the bonding nature from the van der Waals to the covalent potential energy surface is responsible for the conversion of some chemical energy into photon energy with the production of blue-shifted fluorescence. Apparently a similar change in bonding is occurring after the electronic excitation of the triplet dimers.

The (B)$1^1\Pi_u$ and (d)$1^3\Pi_g$ states of K_2 correlate to the K 4P + 4S separated atomic limit and possess the same long-range behavior. If the dissociation of the $1^3\Pi_g$ state produces separated K atoms, it is difficult to understand how they would recombine on the helium cluster to form a (B)$1^1\Pi_u$ state since at 8.1 Å this state possesses a barrier of 295 cm^{-1} above the asymptote.[57] If the cluster contains a third (uncomplexed) K atom, the observation could be explained. However, at this point, the mechanism of the formation of the singlet dimer state from the dissociation of the triplet state cannot be considered fully understood.

Moving on to the heteronuclear dimers, emission spectra recorded by excitation of the NaK transitions would be expected to provide the detailed level structure of the lowest triplet state. In addition to this, we again observe the unusual feature of emission lines ocurring at a greater energy than the excitation position. Unlike the $1^3\Pi_g \leftarrow 1^3\Sigma_u^+$ transition of K_2, the NaK bands under observation here possess bound excited states. Dispersing the fluorescence of the (c)$2^3\Sigma^+ \rightarrow$ (a)$1^3\Sigma^+$ transition produces the spectrum of Figure 16. In addition to the direct fluorescence to the lowest triplet state located to the red of the excitation frequency, a weak fluorescence from the K atomic lines can be seen along with an unresolved Franck−Condon envelope of a singlet molecular band of the NaK molecule. After intersystem crossing, a coupling to a repulsive singlet excited state could lead to fluorescence from a single potassium atom.

Emission after excitation of the (d)$2^3\Pi \leftarrow$ (a)$1^3\Sigma^+$ transition produces fluorescence across a large spectral range, from 10 000 cm^{-1} to greater than 20 000 cm^{-1}. Thousands of overlapping lines are observed across the region. The large density of lines does not allow full assignment of the entire emission spectrum. Instead, modeling using the RKR potential curves allows the identification of the various electronic states that are observed. Figure 17 reveals that, in addition to the resonant triplet fluorescence to the red of the excitation position, the spectrum consists of four singlet bands of the NaK molecule. *All* singlet states below the potential energy of the triplet excited level are present. This includes the A, B, C, and D singlet states. The RKR potentials used as input into the LEVEL 6.0 program[38] to calculate the line positions were derived from refs 52 and 59. Spin−orbit perturbations must allow intersystem crossing from the triplet to the singlet manifold. Again, the greater binding energy of the singlet ground state of the NaK molecule than the lowest triplet state allows the production of blue-shifted fluorescence. The appearance of the atomic potassium fluorescence results from the coupling to nearby repulsive states that dissociate to an excited K atom and a ground state Na. An excitation transfer mechanism between NaK and K atoms which may also be separately present (similar to that observed in the experiments involving Na_2) could also occur. It is assumed that the unusual appearance of singlet transitions resulting from the excitation of the triplet excited states of NaK is a result of the presence of the helium cluster in the spectroscopic probing of the alkali dimer chromophore. Further study of these alkali systems is needed if the properties of helium clusters that induce these spin-changing effects are to be elucidated.

IV. Conclusions

Helium cluster isolation spectroscopy of electronic molecular transitions was originally introduced as a diagnostic tool to study the structure and dynamics of helium droplets in view of their nature of finite size superfluid systems. As a result of the recent work both in our laboratory[17,58] and in Göttingen,[20,21] the great

potential of helium clusters for providing a weakly interacting, cold environment for the formation and spectroscopy of unstable molecules has been established. The investigation of five triplet and one singlet transition in the alkali dimers Li_2, Na_2, K_2, and NaK reported in this paper directly supports this conclusion. While the study of previously known bound−bound transitions helped to describe and understand the method itself, the newly recorded bound−free transitions provide the first experimental data for determining the potentials of some of the repulsive states. Our findings are summarized in the following.

1. The influence of the helium droplet on the spectral position of molecular bands is rather small. Vibrational bands of known Na_2 transitions experience spectral shifts of only 2.8 cm^{-1} to the red ($(A)1^1\Sigma_u^+ \leftarrow (X)1^1\Sigma_g^+$) or 5 cm^{-1} to the blue ($(c)1^3\Sigma_g^+ \leftarrow (a)1^3\Sigma_u^+$) on the cold cluster compared to the gas-phase values. In rare gas matrix isolation spectroscopy, the observed[60] and calculated[61] spectral shifts for the $(A)1^1\Sigma_u^+ \leftarrow (X)1^1\Sigma_g^+$ and $(B)1^1\Pi_u \leftarrow (X)1^1\Sigma_g^+$ systems of Na_2 are much larger, ranging from −400 to 520 cm^{-1} in the case of a solid Kr matrix. Takahashi et al.[62] observed a 700 cm^{-1} blue shift for the $(B)1^1\Pi_u \leftarrow (X)1^1\Sigma_g^+$ transition of Na_2 in liquid helium. Clearly, the surface of large clusters of 0.4 K internal temperature represents an almost nonperturbing substrate for the spectroscopy of molecules that are not solvated by the cluster.

While the vibrational constants of the triplet dimers obtained from the spectra will be slightly altered from their gas-phase values, the spectroscopic shifts are small enough that the data can be used to test the validity of theoretical potential energy curves or extend the body of data previously derived about the state. Therefore, we have attempted to model the $1^3\Sigma_g^+$ excited state of Na_2 using the semiempirical Hartree−Fock damped dispersion (HFD) form. The successful extension of this method from systems such as the noble gas dimers to the alkali dimer excited states, where resonant exchange interactions are present, provides a simple model that can be used to describe potential energy curves for a larger class of systems if the long-range coefficients are known. The universal damping functions for the correlation energy appear to work equally well in both types of systems.

2. The vibrational bands of the singlet molecules are accompanied by a phonon wing extending to the blue of the origin of the transition. A more detailed study of this phonon wing and its dependence on the cluster size should provide information about the surface and bulk excitations of the helium droplet along the line of the work on glyoxal by Hartmann et al.[21] with the advantage that a species located on the cluster surface should be more sensitive than an interior species to changes produced by altering the cluster size.

3. In the cold cluster environment, weakly bound molecules are formed from deposited atoms as proven by the experiment on NaK carried out with separate pick-up regions for sodium and potassium. Moreover, smaller bond energies yield higher survival probabilities for the species formed on the helium cluster. Helium cluster isolation spectroscopy is therefore a method that favors the accumulation of unstable species, and the investigation of their spectra is not obscured by more strongly bound molecules that in other experiments may preferentially form. The availability of a large population of triplet alkali metal dimers provides an alternative to perturbation-facilitated spectroscopy to gain access to the triplet manifold of electronic states.

4. The measurement of nearly unperturbed spectra of weakly bound molecules over a large wavelength range allows rigorous testing of theoretical potentials for van der Waals systems. Examples of this type of work are the $1^3\Pi_g$ states of Li_2 and K_2 and our comparison of measured NaK band positions with values calculated from various theoretical potential energy curves.

In large aggregates, many-body effects are important. They can be accounted for and precisely modeled if the two-body potentials are well-known. Our identification and vibrational analysis of quartet spectra of Na_3 in combination with the triplet two-body potential has revealed the considerable contribution of three-body forces to the overlap repulsion component of the interaction potential of this trimer. Since noble gases, for which the three-body overlap energy is small, and the alkali metals are at the opposite ends of a "hardness" scale for atoms, the stage is now set for a more complete and quantitative look at this area of molecular science. The need for a more complete picture of many-body interactions is still the bottleneck for a better understanding of condensed matter and in particular, solution chemistry.

5. Establishing different concentrations of dopant atoms or molecules in the pick-up region, the size of product aggregates on the helium droplet can be varied. Also, the approximate size of an aggregate giving rise to an unidentified spectrum may be determined by measuring the intensity dependence of this spectrum on the partial pressure of dopants in the pick-up zone. We succeeded in identifying Na_3 and K_3 quartet spectra using this procedure. Visticot et al.[63] doped argon clusters with atoms in a similar pick-up arrangement. In a detailed study of size distributions of molecules formed by these atoms, they varied the pick-up partial pressure over a large range and found that the product sizes followed a Poisson distribution. Bartelt and collaborators have recently succeeded in collecting more than 10 atoms of Ag and In in the same helium cluster.[64] Helium cluster isolation spectroscopy appears to be a promising technique for the study of medium size atomic clusters.

V. Future Directions

Small metal clusters and metal-containing aggregates are usually generated in molecular beams with internal temperatures of several hundred Kelvin. At about 300 K, not even the vibrational structure can be spectrally resolved for alkali clusters[65] and alkali oxide or halide complexes[66] containing four to ten atoms. Ellert et al.[65] showed a significant improvement in resolution when the species were cooled to about 30 K. Small nonstoichiometric alkali halide and oxide clusters[66] as well as small alkali/water clusters attached to helium droplets of 0.4 K temperature will be cold enough to exhibit vibrational structure in their electronic spectra, which so far have not even been resolved for Na_2F. Similar advances should be possible for the spectroscopy of large organic molecules embedded in the helium clusters.[67]

Atoms or molecules residing on the 0.4 K cluster form new complexes only if there is no reaction barrier involved. Theoretically predicted barriers can be tested by depositing the reaction partners with the use of separate pick-up cells and probing the products with spectroscopic methods, allowing the study of phenomena that are important in low-temperature kinetics. Metastable states of reactive molecules and radicals could also be spectroscopically probed. While alkali metal atoms are one-electron systems and show relatively simple electron spin configurations when forming small aggregates, clusters of elements with partially filled p or d shells may occur in weakly bound novel spin states with different bonding schemes that can only be formed and studied in the cold helium cluster environment.

Our experiments have revealed some interesting relaxation processes. More investigations are needed to shed light on the vibrational relaxation of molecules on the cluster surface, on spin conversion processes, on change of bonding nature, and on unimolecular dissociation in the presence of the helium droplet. Many of the planned investigations will be carried out in the time domain using short laser pulses. Another interesting question concerns the equilibrium of different degrees of freedom. Double-resonance experiments involving LIF-detected radio frequency and microwave absorption or IR absorption spectroscopy with bolometric detection can be used to probe the population distribution of electron spin states and rotational or vibrational levels.

It must be emphasized that the helium clusters provide a unique opportunity to study the spectroscopy of small to relatively large molecules in an environment that can produce an ultracold sample, with a lower temperature beyond what may be obtained by conventional molecular beam expansions. Due to the low internal cluster temperature, product molecules are rotationally and vibrationally cold, which simplifies their spectra. In a cluster beam appraratus, all molecular beam spectroscopy methods may be applied. Helium cluster isolation spectroscopy therefore permits infrared absorption,[20,23] optical−optical, laser−microwave, or laser−radio frequency double-resonance techniques, photoionization with mass selective detection, or light or particle scattering. Due to this versatility, it should become an established method complementing the traditional matrix isolation technique. We are aware that these goals cannot be achieved quickly, but the prospects are exciting and full of promise. Helium cluster isolation spectroscopy may open the door to a new chapter of low-temperature chemistry on the microscopic scale.

Acknowledgment. We gratefully acknowledge fruitful discussions with K. K. Lehmann, W. C. Stwalley, and P. Julienne. The latter kindly calculated for us for the first time the $1^3\Pi_g \leftarrow 1^3\Sigma_u^+$ spectrum of Li_2, confirming its assignment to the bound−free transition. We would like to thank R. J. LeRoy for providing the programs to calculate the diatomic spectra. We also thank W. S. Warren for the use of the dye lasers that made these experiments possible. This work was carried out with the support of the AFOSR (HEDM program) under grant F49620-95-1-0086.P0001. M.G. would like to acknowledge support of this work by the Division of Geosciences and Engineering and the Division of Chemical Sciences, both of the Office of Basic Energy Sciences, U.S. Department of Energy. Pacific Northwest National Laboratory is a multiprogram national laboratory operated by Battelle Memorial Institute for the Department of Energy, under Contract No. DE-AC6-76RLO 1830.

References and Notes

(1) Schmidt-Mink, I.; Müller, W.; Meyer, W. *Chem. Phys.* **1985**, *92*, 263.

(2) Magnier, S.; Millé, Ph.; Dulieu, O.; Masnou-Seeuws, F. *J. Chem. Phys.* **1993**, *98*, 7113. Magnier, S.; Millé, Ph. *Phys. Rev. A: Gen. Phys.* **1996** , *54*, 204.

(3) Higgins, J.; Ernst, W. E.; Callegari, C.; Reho, J.; Lehmann, K. K.; Gutowski, M.; Scoles, G. *Phys. Rev. Lett.* **1996**, *77*, 4532.

(4) Roscoe, H. E.; Schuster, A. *Proc. R. Soc. London* **1874**, *22*, 362.

(5) Verma, K. K.; Bahns, J. T.; Rajaei-Rizi, A. R.; Stwalley, W. C. *J. Chem. Phys.* **1983**, *78*, 3599.

(6) Jackowska, I.; Jastrzebski, W.; Feber, R.; Nikolayeva, O.; Kowalczyk, P. *Mol. Phys.* **1996**, *89*, 1719, and references therein.

(7) Tsai, C. C.; Bahns, J. T.; Stwalley, W. C. *Chem. Phys. Lett.* **1995**, *236*, 553, and references therein.

(8) Konowalow, D. D.; Julienne, P. S. *J. Chem. Phys.* **1980**, *72*, 5815.

(9) Breford, E. J.; Engelke, F. *J. Chem. Phys.* **1979**, *71*, 1994.

(10) Huennekens, J.; Schaefer, S.; Ligare, M.; Happer, W. *J. Chem. Phys.* **1984**, *80*, 4794.

(11) Li Li; Rice, S. F.; Field, R. W. *J. Chem. Phys.* **1985**, *82*, 1178.

(12) Yiannopoulou, A.; Urbanski, K.; Lyyra, A. M.; Li Li; Ji, B.; Bahns, J. T.; Stwalley, W. C. *J. Chem. Phys.* **1995**, *102*, 3024.

(13) Kim, J. T.; Wang, H.; Tsai, C. C.; Bahns, J. T.; Stwalley, W. C.; Jong, G.; Lyyra, A. M. *J. Chem. Phys.* **1995**, *102*, 6646.

(14) Färbert, A.; Koch, J.; Platz, T.; Demtröder, W. *Chem. Phys. Lett.* **1994**, *223*, 546. Diemer, U.; Gress, J.; Demtröder, W. *Chem. Phys. Lett.* **1991**, *178*, 330.

(15) Lett, P. D.; Julienne, P. S.; Phillips, W. D. *Annu. Rev. Phys. Chem.* **1995**, *46*, 423.

(16) Doyle, J. M.; Friedrich, B.; Kim, J.; Patterson, D. *Phys. Rev. A: Gen. Phys.* **1995**, *52*, 2515.

(17) Stienkemeier, F.; Ernst, W. E.; Higgins, J.; Scoles, G. *J. Chem. Phys.* **1995**, *102*, 615.

(18) Stienkemeier, F.; Higgins, J.; Ernst, W. E.; Scoles, G. *Phys. Rev. Lett.* **1995**, *74*, 3592.

(19) Stienkemeier, F.; Higgins, J.; Ernst, W. E.; Scoles, G. *Z. Phys. B: Condens. Matter* **1995**, *98*, 413.

(20) Hartmann, M.; Miller, R. E.; Toennies, J. P.; Vilesov, A. *Phys. Rev. Lett.* **1995**, *75*, 1566.

(21) Hartmann, M.; Mielke, F.; Toennies, J. P.; Vilesov, A. F.; Benedek, G. *Phys. Rev. Lett.* **1996**, *76*, 4560.

(22) Brink, D. M.; Stringari, S. *Z. Phys. D: At., Mol. Clusters* **1990**, *15*, 257.

(23) Goyal, S.; Schutt, D. L.; Scoles, G. *Phys. Rev. Lett.* **1992**, *69*, 993. Goyal, S.; Schutt, D. L.; Scoles, G. *J. Phys. Chem.* **1993**, *97*, 2236.

(24) Barnett, R. N.; Whaley, K. B. *J. Chem. Phys.* **1993**, *99*, 9730.

(25) Pascale, J. *Technical Report, Service de Physique des Atoms et des Surfaces* (C.E.N. Saclay, Gif sur Yvette-Cédex, France, 1983).

(26) Anderson, J. B.; Traynor, C. A.; Boghosian, B. M. *J. Chem. Phys.* **1993**, *99*, 345.

(27) Ancilotto, F.; Cheng, E.; Cole, M. W.; Toigo, F. *Z. Phys. B: Condens. Matter* **1995**, *98*, 823.

(28) Stienkemeier, F.; Higgins, J.; Callegari, C.; Scoles, G. *Z. Phys. D: At., Mol. Clusters* **1996**, *38*, 253.

(29) Jones, K. M.; Malecki, S.; Bize, S.; Lett, P. D.; William, C. J.; Richling, H.; Knockel, H.; Tiemann, E.; Wang, H.; Gould, P. L.; Stwalley, W. C. *Phys. Rev. A: Gen. Phys.* **1996**, *54*, R1006.

(30) Friedman-Hill, E. J.; Field, R. W. *J. Chem. Phys.* **1992**, *96*, 2444.

(31) Stringari, S.; Treiner, J. *J. Chem. Phys.* **1987**, *87*, 5021.

(32) Gough, T. E.; Mengel, M.; Rowntree, P. A.; Scoles, G. *J. Chem. Phys.* **1985**, *83*, 4958.

(33) Färbert, A.; Kowalczyk, P.; von Busch, H..; Demtröder, W. *Chem. Phys. Lett.* **1996**, *252*, 243. Färbert, A.; Lutz, J.; Platz, T.; Demtröder, W. *Z. Phys. D: At., Mol. Clusters* **1996** *36*, 249. Färbert, A.; Demtröder, W. *Chem. Phys. Lett.* **1997**, *264*, 225.

(34) Tellinghuisen, J. *J. Mol. Spectrosc.* **1972**, *44*, 194.

(35) Konowalow, D. D.; Rosenkrantz, M. E.; Hochhauser, D. S. *J. Mol. Spectrosc.* **1983**, *99*, 321.

(36) Douketis, C.; Scoles, G.; Marchetti, S.; Zen, M.; Thakkar, A. J. *J. Chem. Phys.* **1982**, *76*, 3057.

(37) Marinescu, M.; Dalgarno, A. *Phys. Rev. A: Gen. Phys.* **1996**, *49*, 982.

(38) LeRoy, R. J. *University of Waterloo Chemical Physics Research Report*, CP-555, 1995.

(39) Scoles, G.; Gutowski, M.; Higgins, J.; Katz, D.; Reho, J. To be published.

(40) Erdman, P. S.; Sando, K. M.; Stwalley, W. C.; Larson, C. W.; Fajardo, M. E. *Chem. Phys. Lett.* **1996**, *252*, 248.

(41) Leroy, R. J. *Comp. Phys. Commu.* **1989**, *52*, 383.

(42) Konowalow, D. D.; Fish, J. L. *Chem. Phys.* **1984**, *84*, 463.

(43) Zemke, W. T.; Stwalley, W. C. *J. Phys. Chem.* **1993**, *97*, 2053.

(44) Pichler, G.; Milosevic, S.; Veza, D.; Beuc, R. J. *J. Phys. B* **1983**, *16*, 4619.

(45) Johnson, D. E.; Eden, J. G. *J. Opt. Soc. Am. B* **1985**, *2*, 721.

(46) Luh, W. T.; Bahns, J. T.; Lyyra, A. M.; Sando, K. M.; Stwalley, W. C. *J. Chem. Phys.* **1988**, *88*, 2235.

(47) Luh, W. T.; Sando, K. M.; Lyyra, A. M.; Stwalley, W. C. *Chem. Phys. Lett.* **1988**, *144*, 221.

(48) Magnier, S. Ph.D. Thesis.

(49) Jeung, G-H.; Ross, A. J. *J. Phys. B* **1988**, *21*, 1473.

(50) Li, L.; Lyyra, A. M.; Luh, W. T.; Stwalley, W. C. *J. Chem. Phys.* **1990**, *93*, 8452.

(51) Kowalczyk, P.; Sadeghi, N. *J. Chem. Phys.* **1995**, *102*, 8321.

(52) Stevens, W. J.; Konowalow, D. D.; Ratcliff, L. B. *J. Chem. Phys.* **1984**, *80*, 1215.

(53) Loomis, F. W.; Arvin, M. J. *Phys. Rev.* **1934**, *46*, 286.

(54) Breford, E. J.; Engelke, F. *Chem. Phys. Lett.* **1978**, *53*, 282.

(55) Kowalczyk, P. *J. Mol. Spectrosc.* **1989**, *136*, 1.

(56) Haberland, H.; in *Clusters of Atoms and Molecules*; Haberland, H., Ed.; Springer Series in Chemical Physics; Vol. 52, p 221.

(57) Heinze, J.; Schühle, U.; Engelke, F.; Caldwell, C. D. *J. Chem. Phys.* **1987**, *87*, 45.

(58) Higgins, J.; Callegari, C.; Reho, J.; Stienkemeier, F.; Ernst, W. E.; Lehmann, K. K.; Gutowski, M.; Scoles, G. *Science* (*Washington, D.C.*) **1996**, *273*, 629.
(59) Kasahara, S.; Baba, M.; Kató, H. *J. Chem. Phys.* **1991**, *94*, 7713.
(60) Hofmann, M.; Leutwyler, S.; Schulze, W. *Chem. Phys.* **1979**, *40*, 145.
(61) Nemukhin, A. V.; Grigorenko, B. L.; Sergeev, G. B. *Can. J. Phys.* **1994**, *72*, 909.
(62) Takahashi, Y.; Sano, K.; Kinoshito, T.; Yabuzaki, T. *Phys. Rev. Lett.* **1993**, *71*, 1035.
(63) Visticot, J. P.; dePujo, P.; Mestdagh, J. M. *J. Chem. Phys.* **1996**, *100*, 158.
(64) Bartelt, A; Close, J. D.; Federmann, F.; Quaas, N.; Toennies, J. P. *Phys. Rev. Lett.* **1996**, *77*, 3525.
(65) Ellert, C.; Schmidt, M.; Schmitt, C.; Reiners, T.; Haberland, H. *Phys. Rev. Lett.* **1995**, *75*, 1731.
(66) Vituccio, D. T.; Hermann, R. F. W.; Ernst, W. E. *J. Chem. Phys.* **1997**, *106*, 3865.
(67) Hartmann, M. Ph.D. Thesis.